MAUSAM, **72**, 3 (July 2021), 553-570

551.577 : 551.501.86 (540.61)

# Study of GPS-retrieved integrated precipitable water over Bangalore

RAJASRI SEN JAISWAL, MUKUNDAN M., THIRUMALA LAKSHMI K.,

RICHA DOBAL and SIVA M.

*Centre for Study on Rainfall and Radio wave Propagation*

*Sona College of Technology, Salem – 636 005, Tamil Nadu, India*

(*Received 6 October 2020, Accepted 15 June 2021*)

**e mails : rajasrisenjaiswal@gmail.com; rajasrisenjaiswal@sonatech.ac.in**

सार – इस शोध पत्र में, लेखकों ने वर्ष 2016 के लिए ग्लोबल पोजिशनिंग सिस्टम (GPS) से प्राप्त क्षोभमंडलीय शीरोबिंदु विलंब (TZD) से बैंगलोर में समेकित वर्षणीय जल वाष्प (IPWV) का अनुमान लगाने का प्रयास किया है। इस तरह से आकलित कुल वर्षणीय जल वाष्प (IPWV) से दैनिक, दैनिक और मासिक बदलाव का पता चलता है। TZD के दैनिक, दैनिक और मासिक रूपांतर, शीरोबिंदु आर्द्र विलंब (ZWD), भारित माध्य तापमान (Tm), और Π भी प्रस्तुत किए गए हैं। इस शोध पत्र का उद्देश्य विशेष रूप से आईपीडब्ल्यूवी के नियंत्रण कारकों का पता लगाना है। इस उद्देश्य के लिए, लेखकों ने कुछ मौसम संबंधी तत्वों की जांच की है, जैसे, सतह का तापमान, दबाव, सापेक्ष आर्द्रता और कुल सौर विकिरण (TSI)। अध्ययन से पता चलता है कि ये प्राचल एक साथ समेकित वर्षणीय जल वाष्प (IPWV) को नियंत्रित करते हैं।

**ABSTRACT.** In this paper, the authors have attempted to estimate integrated precipitable water vapor (IPWV) over Bangalore from the troposphericzenith delay (TZD) obtained from the Global Positioning System (GPS) for the year 2016. The IPWV so estimated shows diurnal, daily and monthly variations. The diurnal, daily and monthly variations of TZD, zenith wet delay (ZWD), weighted mean temperature (Tm) and Π have also been presented. The paper aims in particular, to find out the controlling factors of IPWV. For this purpose, the authors have investigated a few meteorological elements, *viz*., surface temperature, pressure, relative humidity and also total solar irradiance (TSI). The study shows that these parameters put together control IPWV.

**Key words** – Global Positioning System, Integrated precipitable water, Total solar irradiance, Zenith wet delay.

## 1. Introduction

Rain is one of the major factors that control the livelihood on Earth, impacting its socio-economic arena. Therefore, understanding rainfall dynamics remains one of the topmost priorities. Several places on Earth are witnessing a change in rainfall patterns due to climate change. Therefore, awareness of impending rainfall dynamics due to climate change must be discerned.

The precipitable water is a parameter that governs rainfall. The precipitable water is the amount of precipitation that would fall on the ground if the entire water vapor in the vertical column would condense (Max, 2001), while precipitation water (PW) (TRMM Data Users Handbook, 2001) is the actual amount of moisture that has precipitated as rain. A study by Sen Jaiswal *et al*. (2014) shows that the precipitation water at the peak cloud liquid water can explain the crests and troughs of rainfall time series. The study (Sen Jaiswal *et al*., 2014) also shows that a high value of total precipitation water ensures high rainfall, while a less quantity of precipitation water leads to less rainfall, indicating that the precipitation water is a direct measure of rainfall, as the temperature is a direct measure of heat. The precipitable water, which is the moisture present in the atmosphere, absorbs both the long-wave and short-wave radiation. Thus, it affects the emissivity of clouds (Taylor and Ghan, 1992) and plays a significant role in cloud formation. Battan and Kassander (1960) have identified precipitable water as a key factor in convective cloud formation. It is also a significant parameter to characterize a stratiform and convective cloud. Sen Jaiswal *et al*. (2020b) have found that the precipitation water in a convective cloud is significantly higher than that in a stratiform cloud. Besides, the amount of water vapor present in the atmosphere provides information about the latent heat absorbed and evolved at different levels. Thus, it plays a very important role in the radiation budget of the Earth-atmosphere system. The rainfall in the Indian subcontinent during the summer monsoon months primarily depends on the moisture transported from the Arabian Sea and the Bay of Bengal (Mohanty *et al*., 1994; Webster *et al*., 1998). During the winter monsoon, the rainfall received on the East coast of India is due to the moisture-laden air blowing from the Bay of Bengal. It is noteworthy that India receives more

rainfall during the summer monsoon than the winter monsoon. A study by Durai *et al*. (2007) indicates that the spatial and temporal distribution of precipitable water can predict monsoon over India. A study (Kuo *et al*., 1993) indicates that precipitable water as an input to the numerical weather model improves precipitation forecast. Thus, it appears that the moisture content of the air is one of the parameters that determine the amount of rainfall. A study (Junker, 2008) indicates the dependence of rainfall intensity on the vertical moisture flux present in the cloud. The annual cycle of precipitable water over Lisbon in 2012 correlates positively with the probability of extreme rainfall (Benevides *et al*., 2015).

By realizing the fact that precipitable water is of immense importance in climate study, it is necessary to recognize the meteorological elements that control it. Several researchers all over the globe have tried to find out the controlling factors of precipitable water. A study over China (Zhai and Eskridge, 1997) revealed that atmospheric precipitable water is related to surface temperature. Choudhary (1996) has found relative humidity a significant indicator of total precipitable water. The study of Mishra (2019) over India has indicated a strong dependence of increased integrated precipitable water on warming. A study (Fujita and Sato, 2017) over Japan analyzed the relation between the surface temperature and precipitable water vapor derived from GPS. The study (Fujita and Sato, 2017) shows that the vertical distribution of water vapor is a function of surface temperature. A study (Varma Raja *et al*., 2007) showed that the mean differential precipitable water (GPS-AIRS) linearly varies with surface pressure. Kruczyk (2015) reported that the differential integrated precipitable water vapor (GPS-sunphotometer) is a function of surface temperature and season. Investigations indicate a positive correlation between the precipitable water vapor and rain, but point out that not all precipitable water vapor peaks lead to precipitation (Champollion *et al*., 2004; Bastin *et al*., 2007; Yan *et al*., 2009; Brenot *et al*., 2014). A study in Japan (Shoji, 2013), shows that when the precipitable water reached a certain threshold value as a function of the surface temperature, the precipitation frequency increased.

Measuring precipitable water and investigating its variability is of immense importance. The radiosondes provide precipitable water in the atmosphere. Although Eliott (1995) argues that the radiosonde data are affected by poor quality and issues of calibration, these have been the standard and reliable sources of upper air atmospheric elements data. However, because of practical difficulties of launching these instruments, particularly from large oceanic areas and the relatively higher cost of consumables involved for collecting data from a number of locations, these data are not available at a greater temporal and spatial resolution. Over some stations, the data are available at 0000 hr and 1200 hr. Over a few selected locations, these are available at an interval of three hours. On the other hand, satellite-based precipitable water retrievals have far better spatial and temporal resolutions. The Tropical Rainfall Measuring Mission satellite (TRMM) provides the precipitation water with a very good spatial resolution. But, over a location, the values are obtained only once, or rarely, twice a day. Besides, the Tropical Rainfall Measuring Mission satellite (TRMM) gives precipitation water during rainy conditions only. Hence, the search for a device that gives precipitation water in both rainy and non-rainy conditions, with a better spatial and temporal resolution turns one's attention to the Global Positioning System (GPS), which measures integrated precipitable water vapor (IPWV) both in rainy and non-rainy conditions. The spatial resolution of GPS-retrieved IPWV, the total signal delay and the wet delay is 0.001 m (NOAA, 2021). The temporal resolution of GPS-retrieved parameters is 2 hours. This is of immense help in investigating the precipitable water during the pre-monsoon, monsoon and post-monsoon seasons of India.

However, there are a few limitations with the GPS-based precipitable water estimation. Kruczyk (2015) has shown that the precipitable water measured by a sunphotometer is less than that measured by GPS. Dutta *et al*. (2014) reported an underestimation of GPS-retrieved precipitable water over the radiosonde radio wind (RSRW)-retrieved values. Brenot *et al*. (2006) reported an underestimation of zenith wet delay and precipitable water in strong convective cells, due to an overestimation of zenith hydrostatic delay caused by ice particles. Benevides *et al*. *(*2015) found that some of the mismatches between precipitable water vapor data and precipitation may be because of a relatively sparse rain gauge network that missed recording many of the rainy events. However, they (Benevides *et al*., 2015) reported that most of the mismatches between the rainfall and precipitable water vapor are likely due to the 3-D nature of the precipitable water vapor, which cannot be detected by a single GPS receiver. Besides, the error in position estimation due to antenna scattering effects and multipath effects also lead to an error in integrated precipitable water estimation (Emardson *et al*., 1998; Champollion *et al*., 2004). Solheim *et al*. (1999) opine that the multipath effect is one of the major factors contributing to the error in precipitable water estimation. They stated that antenna design can reduce the error caused by the multipath effect. Baelen *et al*. (2011) have reported that the hail, fog, or dew also affect the measurements of the integrated water vapor. Puviarasan *et al*. (2020) have reported under estimation of GPS-retrieved precipitable water in a narrow

convective cloud. They (Puviarasan *et al*., 2020) opine that the underestimation occurred because of the non-availability of GPS satellites in the vicinity of the zenith direction. To achieve better accuracy of precipitable water estimation for narrow convective clouds, they suggest simultaneous observations by other constellations along with GPS. Shoji (2013) opines that the use of GPS precipitable water vapor data with other meteorological elements will improve the performance of GPS meteorology. Solheim *et al*. (1999) opine that the error in atmospheric delay, which is used to estimate precipitable water from GPS, can be reduced by using pointed radiometers and by modeling. Maorong *et al*. (2000) propose a strategy that reduces the effect of satellite orbit errors on zenith delay measured by the satellites in the GPS constellation. They opine that the Keplerian parameters of the satellite orbit, *viz*., the semi-major axis, inclination and argument of perigee pose a significant error in the estimation of tropospheric zenith delay.

In this paper, the authors have investigated GPS-based integrated precipitable water vapor (IPWV) over Bangalore, India. They aim to investigate its variability over the monsoon months. The authors aim in particular, to find out the factors that control the precipitable water. In an attempt to seek the key parameters controlling the precipitable water, in this paper, the authors have investigated its dependence on a few meteorological elements, *viz*., surface pressure, surface temperature and relative humidity. Besides, in the investigation, they have introduced another parameter, called the total solar irradiance (TSI). The total solar irradiance (TSI) is the solar radiation received at the top of the atmosphere. It is expressed in watt/m$^2$. Studies show that all the meteorological elements follow the solar cycle. Many studies (Arnold and Robinson, 1998; Eddy, 1980; Engels and Geel, 2012) have demonstrated the role of the Sun in influencing the weather and climate on the Earth. Theophrastus (371-287 BCE) had suggested a connection between the rain and sunspots. The north-south movement of the intertropical convergence zone (ITCZ) (Byrne *et al*., 2018) the rise and fall of temperature over a location (Solheim *et al*., 2012), the march of the bright band intensity belt (Sen Jaiswal *et al.*, 2020a) and the occurrence of El Nino and La Nina (Sen Jaiswal *et al*., 2020c), etc. follow the solar cycle. Soon and Yaskell (2003) suggested a correlation between sunspots and wind. Jagannathan and Bhalme (1973) have shown that the characteristics of monsoon circulation and periodicity of rainfall follow the periodicity of sunspots. Haigh (2003) has found that the Sun affects the Earth's climate. Shapiro (1975) has demonstrated the relation between the solar cycle and meteorological elements.

Authors have attempted to estimate the precipitable water over Bangalore, India from the Global Positioning System (GPS) datafor the year 2016. The retrieval of precipitable water from GPS is not a direct one. It is estimated from the error that the precipitable water incorporates in the position estimation of the receiver. The GPS receiver, as a deliverable, measures the phase of the signal transmitted from the satellite. The phase of the transmitted signal as measured by the receiver is not the actual phase of the transmitted signal, rather it is an overestimation. The overestimation of the phase of the transmitted signal is due to the additional path length introduced in the signal during its journey from the satellite transmitter to the receiver on the ground. Several factors, such as the ionospheric delay, the tropospheric delay, the satellite clock offset, the receiver clock offset, the multipath effect, the satellite orbital error and the receiver antenna phase center variation, contribute to the additional path length (Bidikar *et al*., 2014).

When the transmitted signal from the satellite propagates through the atmosphere, the refractive index of the troposphere being slightly greater than unity (*i.e*., that of vacuum), slows down as the refractive index is given by,

$$n = c/v \tag{1}$$

where, $c$ is the velocity of light and $v$ is the velocity of the signal in the medium having refractive index $n$.

So, the signal reaches the receiver late as compared to the time it would reach if it would pass through a vacuum. This adds an extra path length, which changes the phase. Besides, due to the non-uniform refractive index of the troposphere, the signal suffers refraction and it bends more and more as it comes closer to the receiver. This phenomenon also adds to an increased path length. The extra path length posed to the signal, or the change in phase contributed by the troposphere is called a tropospheric delay. The tropospheric delay is expressed in meters. The tropospheric delay is a sum of the hydrostatic delay and the wet delay. The hydrostatic delay is due to the gases present in the atmosphere and the water vapor present in the atmosphere causes the wet delay.

The GPS gives the tropospheric zenith delay (TZD). The zenith hydrostatic delay (ZHD), which is a function of latitude, altitude and surface pressure at the location, is subtracted from the tropospheric zenith delay (TZD) to get the zenith wet delay (ZWD). Zenith wet delay (ZWD) is caused due to precipitable water. Next, the weighted mean temperature ($T_m$) and Π are calculated (Davis *et al.*, 1985) using the values of meteorological elements at different levels in the atmosphere. At last, integrated precipitable

water (IPWV) is calculated by multiplying Π by the zenith wet delay (ZWD).

The Global Positioning System (GPS) is a navigation system that provides a three-dimensional user position (*X*, *Y*, *Z*), time and velocity on or above the Earth's surface. The GPS consists of a space segment, control segment and user segment (Global Positioning System Standard Positioning Service Signal Specification, 1995). The space segment consists of a constellation of 32 satellites. The GPS has been launched by the United States of America on 13$^{th}$ January, 1980. So, the GPS week starts on 13$^{th}$ January, 1980. Thus, the corresponding GPS week on 1$^{st}$ January, 2006 is 1356. The GPS day on a particular date in a year is calculated considering 1$^{st}$ January of the year as GPS day. Thus, 13$^{th}$ February is the 44$^{th}$ GPS day.

## 2. Data and methodology

To study the precipitable water over Bangalore for 2016, first the tropospheric zenith delays (TZD) have been estimated using the Global Positioning System (GPS). GPS provides data every two hours a day. The GPS data over Bangalore, obtained from the International GNSS Service (IGS) have been processed using GAMIT and then integrated precipitable water vapor (IPWV) has been obtained. In this paper, the IPWV so obtained by processing the GPS data using GAMIT is termed as $IPWV_{GPS}$. GAMIT uses a static surface temperature (T), surface pressure (P) and relative humidity ($r_h$). However, these parameters vary and are not at all static over a location. Thus, the authors have attempted to estimate the IPWV over Bangalore, using the actual values of pressure, temperature, relative humidity and the GPS-retrieved tropospheric zenith delay (TZD). They have estimated the IPWV using MATLAB. The IPWV so estimated is termed as $IPWV_{EST}$. The $IPWV_{EST}$ values are available at 0000 hr and 12 hr.

The total solar irradiance (TSI) data for the year 2016 have been obtained from the Solar Radiation and Climate Experiment (SORCE), University of Colorado, Boulder (SORCE, 2019). The TSI values are available once a day. The values of surface temperature, surface pressure and relative humidity are obtained from the Integrated Global Radiosonde Archive (IGRA, 2021). These values are available twice a day.

### 2.1. *Pre-processing of GPS receiver data*

The pre-processing of GPS receiver data using GAMIT is achieved by the following command :

Sh_gamit-expt name-d year gps date. The pre-processing of GPS data includes the conversion of input files (Herring *et al*., 2018), *i.e*., the RINEX file, navigation file and the orbital file to the output Z files using GAMIT. The *Z* files contain the date, time and PRN number of overhead satellites. The *Z* files also contain information on pressure, temperature, the water vapor pressure at the receiver location; the dry zenith delay, *i.e*., the zenith hydrostatic delay (ZHD); zenith wet delay (ZWD); tropospheric zenith delay (TZD); slant wet delay; slant dry delay; total slant delay; dry and wet mapping function. It is noteworthy that the pressure and temperature values derived from the *Z* file are static, *i.e*., these values are not the actual values at an instant. Thus, to estimate the correct IPWV, one needs to use the actual pressure and temperature over a location.

### 2.2. *Post-processing of GPS data*

Post-processing of GPS data includes the conversion of Z files into met files. The Z files are converted into met files by using the command :

Sh_metutil–f oexpta.GPS date–z ziisc. GPS date. For example, Sh_metutil–f oexpta.219–z ziisc. 219. Here "219" represents GPS day. After operating the command, a met file of the form : met_stnname. yr GPS date is obtained. The met files are available every two hours a day. The met file contains all parameters of the z files. Besides, these contain Sig Zen, Sig PW, Grad NS, Grad EW and Sig EW (Herring *et al.*, 2017). Sig Zen is the uncertainty of ZWD, in mm; Sig PW is the uncertainty of PW, in mm; Grad NSA is the N-S component of the gradient of TZD, in mm; Sig NS is the uncertainty of Grad NS, in mm; Grad EW is the East-West component of gradient of TZD, in mm; Sig EW is the uncertainty of Grad EW, in mm.

### 2.3. *Estimation of integrated precipitable water (IPWV) from GPS*

To find the integrated water vapor over a location, one needs the knowledge of several atmospheric parameters, *viz*., surface temperature (*T*); the temperature at the $i^{th}$ level ($T_{di}$); surface pressure (*P*); liquid water density (ρ); saturation vapor pressure ($P_{si}$) at the $i^{th}$ level in the atmosphere; partial vapor pressure at the $i^{th}$ level ($P_{vi}$); relative humidity ($rh_i$); weighted mean temperature ($T_m$); specific gas constant of water ($R_v$); the constants $k_1$, $k_2$, $k_3$; the ratio of molar mass to dry air mass (m); zenith hydrostatic delay (ZHD) and zenith wet delay (ZWD).

The IPWV has been derived from GPS using GAMIT ($IPWV_{GPS}$). The IPWV ($IPWV_{EST}$) has also been estimated over Bangalore, using the troposphericzenith delay (TZD), obtained from GPS; and by calculating zenith hydrostatic delay (ZHD) from the actual pressure,

temperature and height of Earth's station (Elgered *et al.*, 1991); and the zenith wet delay (ZWD), for the year 2016, by using equations (2)-(8).

$$\text{ZHD} = 2.2778\ \text{P} / [1 - 0.00266 \cos(2\lambda) - 0.00028\ \text{H}] \quad (2)$$

where, P is the surface pressure, $\lambda$ is the latitude of Earth's station and H is the height of the station from mean sea level.

While estimating the IPWV using the TZD derived from the GPS, at first, the ZHD has been estimated by using the surface pressure data as recorded by the instruments in the observatory at Bangalore from where radiosondes are launched at 0000 hr and 1200 hr and by using equation (2). The surface pressure data have been obtained from the Integrated Global Radiosonde Archive (IGRA, 2021). Then, the zenith wet delay (ZWD) has been estimated as

$$\text{ZWD} = \text{TZD} - \text{ZHD} \quad (3)$$

The saturation vapor pressure ($P_{si}$) has been estimated using the relation (Davis *et al*., 1985)

$$P_{si} = 6.11 \times 10^{\left(\frac{7.5 \times Td_i}{237.3 + Td_i}\right)} \quad (4)$$

where, $T_{di}$ is the temperature in °C at the $i^{th}$ level in the atmosphere.

The partial vapor pressure ($P_{vi}$) at the $i^{th}$ level has been estimated using the relation (Davis *et al*., 1985)

$$P_{vi} = \frac{rh_i \,.\, P_{si}}{100} \quad (5)$$

where, $rh_i$ is the relative humidity at the $i^{th}$ level.

The weighted mean temperature ($T_m$) has been estimated (Davis *et al.*, 1985) using the relation

$$T_m = \frac{\sum_{i=1}^{N} \frac{P_{vi}}{T_i} \Delta z_i}{\sum_{i=1}^{N} \frac{P_{vi}}{T_i^2} \Delta z_i} \quad (6)$$

where, $i$ denotes the $i^{th}$ level in the atmosphere and $N$ is the number of levels used for estimating $T_m$. $\Delta z_i$ denotes the difference of height between the surface and the $i^{th}$ level.

Next, the proportionality constant $\Pi$ is found out using the relation (Davis *et al*., 1985)

$$\Pi = \frac{10^6}{\rho R_v \left(\frac{K_3}{T_M} + K_2^{'}\right)} \quad (7)$$

where, $\rho$ is the liquid water density at the surface.

$K_2^{'}$ = 22.1 ± 22 * $10^{-2}$ $kPa^{-1}$ (Manandhar *et al*., 2017); $K_3$ = 3.739 ± 0.012 * $10^3$ $k^2Pa^{-1}$ (Manandhar *et al*., 2017); $R_v$ is the water vapor gas constant. Next, the IPWV has been estimated (Askne and Nordius, 1987) using equation (8).

$$\text{IPWV} = \Pi \times \text{ZWD} \quad (8)$$

The IPWV estimated in this paper is the total columnar water vapor from the Earth's surface up to 500 hPa.

Once the integrated precipitable water (IPWV), the tropospheric zenith delay (TZD) and the zenith wet delay (ZWD) are obtained from the GPS every two hours, the values at 0000 hr and 1200 hr are collected for the investigation. These parameters at other times of the day are not included in the study because the surface meteorological elements are available only at 0000 hr and 1200 hr. To investigate the daily variation of a parameter, the values of a particular parameter are plotted against the number of days in a month. The daily variations of the parameters in 2016 are investigated at both 0000 hr and 1200 hr.

To study the monthly variation of these parameters, the monthly averages of a particular parameter were obtained from the daily values.

The authors attempted to find out the functional relationship between the IPWV and the meteorological elements, *viz*., surface pressure, surface temperature, relative humidity and total solar irradiance. For this purpose, they have fitted the IPWV and the meteorological parameters to the linear regression technique. The validity of the model is judged by the *F*-test at a 5% level of significance. In the same manner, the functional relation at 1200 hr is obtained.

The dependence of IPWV on the meteorological parameters has been found out in the following manner : at first, the parameters have been entered into the curve estimation, one by one, considering the IPWV as the dependent variable and the other parameters as an

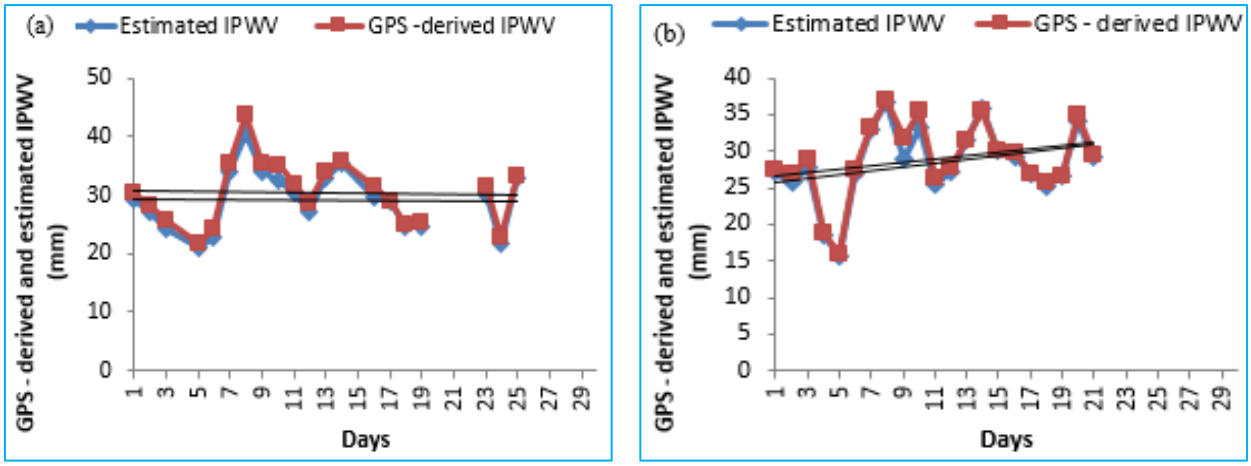


**Figs. 1(a&b).** Daily variation of GPS-derived and estimated IPWV over Bangalore in April 2016 at (a) 0000 hr and (b) 1200 hr

independent one. Next, the dependence was tested by linear regression- considering the IPWV as the dependent one and a combination of any two parameters as the independent variables. In the next stage, a combination of three parameters entered into the linear regression as the independent variables. In the last stage, all four parameters, *viz*., surface pressure, surface temperature, relative humidity and total solar irradiance entered into the linear regression as independent variables, while the IPWV was considered the dependent one.

## 3. Results and discussions

### 3.1. *Comparison between $IPWV_{GPS}$ and $IPWV_{EST}$*

The GPS-derived Integrated Precipitable Water Vapor ($IPWV_{GPS}$) shows a good match with the estimated IPWV ($IPWV_{EST}$). The comparison between the two is shown in Figs. 1(a&b) for April 2016 at 0000 hr and 1200 hr, respectively. Figs. 1(a&b) show that the two match very well. Results for other months are not shown. The error by assuming the estimated value as the standard one varies between 0.03% - 62.75% for the entire year 2016.

The analysis in whole 2016 shows less than 10% error in 92.01% cases at 0000 hr and 98.08% cases at 1200 hr. An error of 30% or greater exists in 0.38% cases at 1200 hr and in no cases at 0000 hr. It is noteworthy that in 32.27% of cases at 0000 hr and 70% cases at 1200 hr, the error was less than 5.0%. The average error is 6.22% and 4.32% at 0000 and 1200 hr, respectively. The range of error at 0000 hr is from 0.05%-26.47%, while at 1200 hr, it varies from 0.03%-62.75%.The maximum error of 62.75% at 1200 hr, occurred only on 13 March. The maximum error of 26.47% at 0000 hr happened on 2 February.

To find the reason for large errors on these two days, the authors compared the values of IPWV. They found that at 0000 hr on 2 February 2016, the IPWV retrieved from the radiosonde, GPS and that estimated were 6.53 mm, 6.8 mm and 5.38 mm, respectively. Thus, the IPW over Lamont, Oklahoma retrieved from GPS was closer to the radiosonde-retrieved value. On 13 March 2016, at 1200 hr, the estimated value (37.32 mm) was close to the radiosonde-retrieved value (36.73), while the GPS-retrieved value was much less (13.9 mm). The reason for such a small $IPWV_{GPS}$ on 13 March 2016 is not known yet. It is noteworthy that in March rainfall is scanty over Bangalore. So, it is very unlikely that the underestimation is due to the inability of GPS receivers to view the cloud.

### 3.2. *Diurnal variation of $IPWV_{EST}$*

The authors have attempted to find out whether the IPWV is higher at 1200 hr than that at 0000 hr. For this purpose, the diurnal variations of IPWV values ($IPWV_{EST}$) estimated at 0000 hr and 1200 hr have been studied. The study reveals that IPWV shows diurnal variations. The study shows that in 2016, in January, May, June, July, August and September, the $IPWV_{1200hr} > IPWV_{0000hr}$ in 71.4%, 79.1%, 76%, 89.5%, 89.9% and 66.6% cases, respectively (results not shown). In March, April, November and December, the $IPWV_{1200hr} > IPWV_{0000hr}$ in 50%, 35.27%, 52.2% and 59.2% cases, respectively (results not shown). The $IPWV_{1200hr} > IPWV_{0000hr}$ in 69.1% cases in 2016. Thus, the result implies that in most of the cases, $IPWV_{1200hr} > IPWV_{0000hr}$. The differential temperature and relative humidity at these two hours appear to cause the differential IPWV. The study further shows that in the year 2016, the $IPWV_{GPS}$ maxima mostly occurred at 14-18 hr (results not shown).

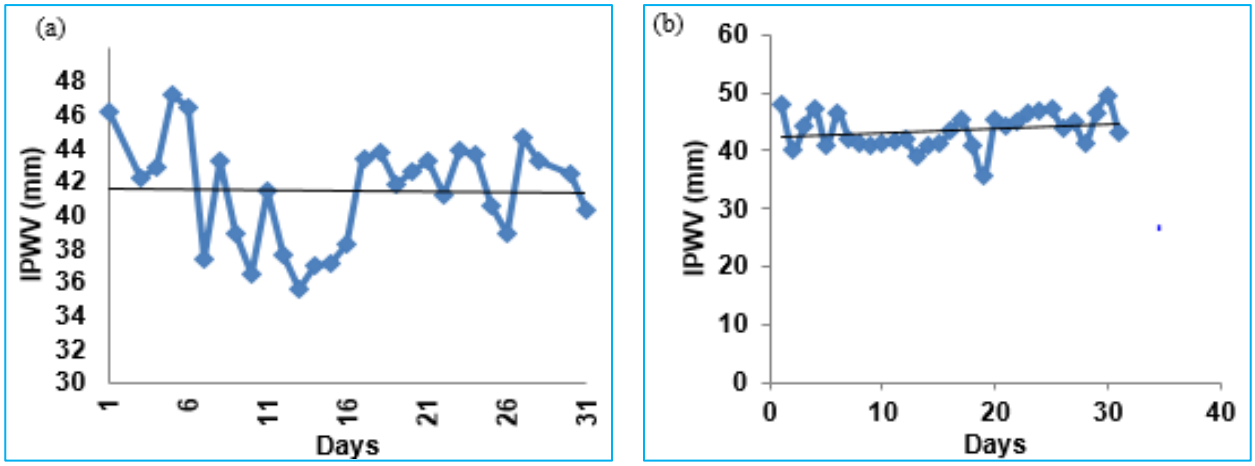


**Figs. 2(a&b).** Daily variation of IPWV over Bangalore in July 2016 at (a) 0000 hr (b) 1200 hr

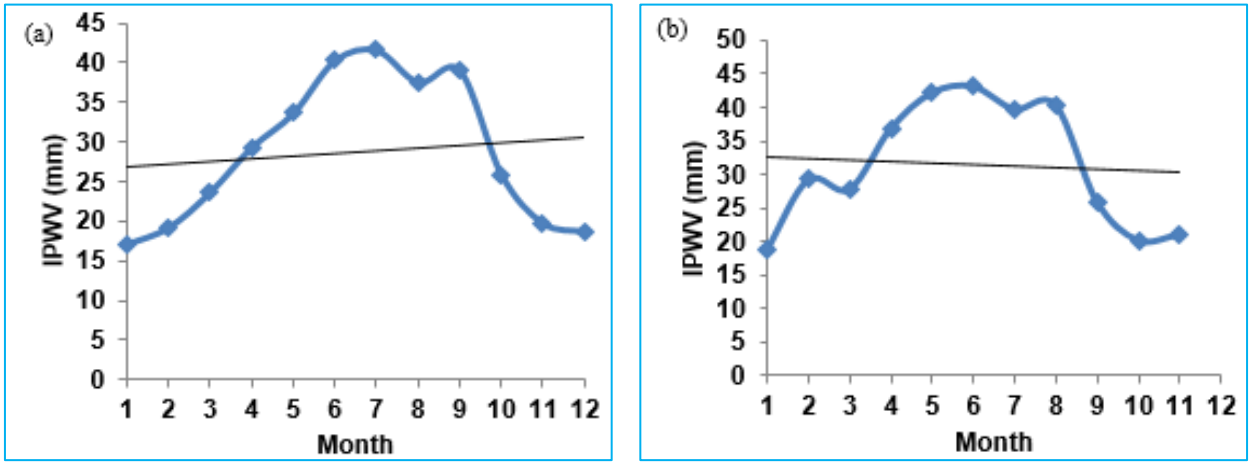


**Figs. 3(a&b).** Monthly variation of IPWV over Bangalore at (a) 0000 hr and (b) 1200 hr

### 3.3. *Daily variation of $IPWV_{EST}$*

Figs. 2(a&b) respectively show the daily variations of IPWV in July 2016, at 0000 hr and 1200 hr. Results for other months are not shown. Figs. 2(a&b) show that IPWV shows significant daily variations. In 2016, the daily IPWV has attained its maximum value of 47.21 mm in July, while the minimum is observed in February at 0000 hr (result not shown). At 1200 hr, the daily maximum IPWV occurred in June, while the minimum occurred in December (result not shown). Thus, the IPWV is more in the summer and less in the winter. The investigation further shows that the daily IPWV showed its peak in June, while the minimum value occurred in February (results not shown).

The study also shows the daily trend of IPWV in a month. It reveals that in 2016, it shows an increasing trend in July. It shows an increasing trend in January-September both at 0000 hr and 1200 hr and a decreasing trend during October-December. In May, it shows an insignificantly decreasing trend (results not shown).

The precipitable water over a location depends on the meteorological elements, *viz*., temperature, pressure, relative humidity on the surface and up in the troposphere. As the meteorological elements vary from time to time, the precipitable water inevitably shows diurnal, daily and monthly variations. A study by Sen Jaiswal *et al*. (2020d) reveals that the IRNSS (Indian Regional Navigation Satellite System)-retrieved total slant delay,

**TABLE 1**

**Date of occurrence of monthly maximum/minimum TSI, TZD & IPWV – 2016**

| Month | Date of occurrence | | Date of occurrence of $IPWV_{EST}$ | | | | Date of occurrence of TZD | | | | Date of occurrence of $IPWV_{GPS}$ | |
|---|---|---|---|---|---|---|---|---|---|---|---|---|
| | | | $IPWV_{mx}$ | | $IPWV_{mn}$ | | $TZD_{mx}$ | | $TZD_{mn}$ | | | |
| | $TSI_{mx}$ | $TSI_{mn}$ | 0000 hr | 1200 hr | 0000 hr | 1200 hr | 0000 hr | 1200 hr | 0000 hr | 1200 hr | $IPWV_{mx}$ | $IPWV_{mn}$ |
| Jan | 1st | 31st | 20th | 19th | 2nd | 5th | 20th | 23rd | 5th | 31st | 20th | 5th |
| Feb | 1st | 29th | 18th | - | 2nd | - | 18th | 17th | 3rd | 2nd | 18th | 3rd |
| Mar | 1st | 31st | 14th | - | 27th | - | 14th | 13th | 27th | 8th | 14th | 13th |
| Apr | 1st | 30th | 8th | 8th | 5th | 5th | 8th | 22nd | 27th | 5th | 8th | 22nd |
| May | 1st | 31 st | 17th | 18th | 24th | 23rd | 19th | 18th | 1st | 23rd | 20th | 24th |
| Jun | 1st | 30th | 11th | 8th | 2nd | 18th | 23rd | 8th | 2nd | 18th | 11th | 2nd |
| Jul | 31st | 3rd | 5th | 30th | 13th | 19th | 5th | 30th | 13th | 19th | 5th | 13th |
| Aug | 31 st | 1 st | 30th | 28th | 2nd | 9th | 26th | 28th | 17th | 20th | 30th | 20th |
| Sep | 30th | 1 st | 22nd | 23rd | 7th | 10th | 22nd | 6th | 7th | 9th | 22nd | 7th |
| Oct | 31 st | 1 st | 12th | 11th | 29th | 26th | 12th | 11th | 24th | 26th | 12th | 24th |
| Nov | 30th | 1 st | 1 st | 1st | 25th | 24th | 1st | 1st | 25th | 27th | 1 st | 25th |
| Dec | 31 st | 1 st | 3rd | 12th | 23rd | 24th | 13th | 12th | 11th | 10th | 3rd | 23rd |

which is caused due to the presence of precipitable water (Emardson and Derks, 2000) in the atmosphere, shows diurnal, daily and monthly variations.

### 3.4. *Monthly variation of $IPWV_{EST}$*

The monthly variation of IPWV in 2016 at 0000 hr and 1200 hr is shown in Figs. 3(a&b), respectively.

Fig. 3(a) shows that over Bangalore, at 0000 hr, the monthly average maximum IPWV of 41.42 mm occurred in July, while the minimum of 16.85 mm happened in January. Fig. 3(b) shows that at 1200 hr, the monthly average maximum (minimum) IPWV of 43.47 mm (19.21 mm) occurred in June (January). In 2016, the monthly average IPWV was higher at 1200 hr than at 0000 hr in January, March, May, June, July, August, September and October-December. In April, it was higher at 0000 hr. The highest values of IPWV ($IPWV_{mx}$) over Bangalore occurred during the S-W monsoon season, *i.e.*, during June-September.

The date of occurrence of maximum IPWV ($IPWV_{mx}$) and minimum IPWV ($IPWV_{mn}$) in 2016 is shown in Table 1 which shows that during January, August and September, the $IPWV_{mx}$ occurred by the end of the month. The investigation at 0000 hr reveals that in February, March, May, June and October, it occurred in the middle of the month and at the beginning of the month in April, July, November and December. The $IPWV_{mx}$ exhibits the same results at 1200 hr, except in December and July. The $IPWV_{mx}$ in July at 1200 hr occurred at the end of the month and in the middle of the month in December.

The $IPWV_{mn}$ at 0000 hr, occurred by the end of the month during October-December, May and March; and at the beginning of the month in January, February, April, June, August and September. The $IPWV_{mn}$ exhibits the same results at 1200 hr, except in June when it occurs on the last day of the month.

Table 1 also shows the dates of occurrence of a few more parameters, like the total solar irradiance (TSI) and the tropospheric zenith delay (TZD), which will be discussed in sections 3.9 and 3.10.

### 3.5. *Validation of $IPWV_{EST}$ against ground truth*

The authors attempted to validate the estimated IPWV with the radiosonde-retrieved precipitable water. The investigation reveals that the error by assuming the radiosonde-retrieved precipitable water as the standard one varies between 0.00% - 75.76% for the entire year 2016.

The analysis in whole 2016 shows less than 10% error in 64.61% cases at 0000 hr and 52.76% cases

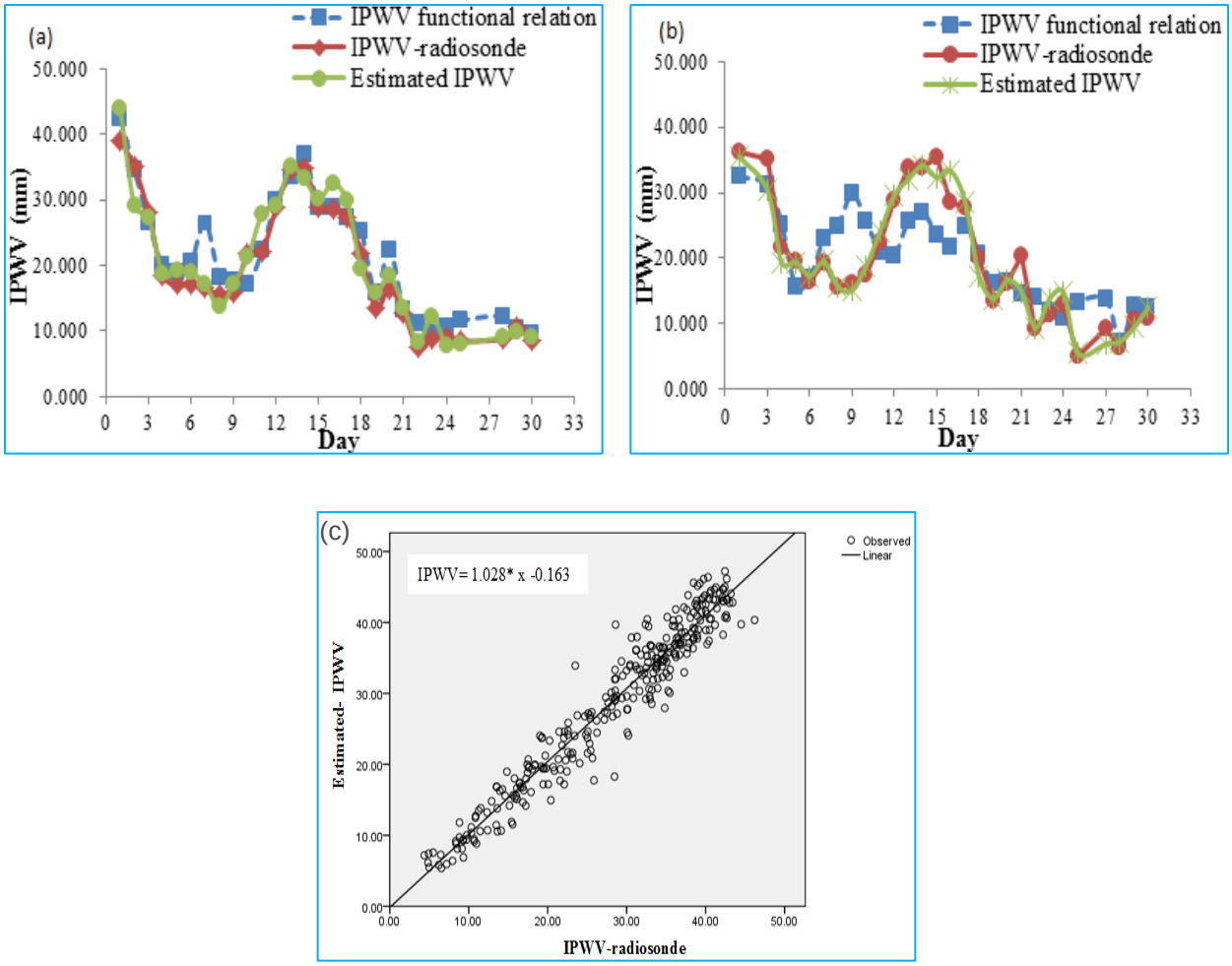


**Figs.4(a-c).** Variation of IPWV-radiosonde, estimated IPWV and functional relation based IPWV over Bangalore in 2016 at (a) 0000 hr, (b) 1200 hr and (c) Variation of IPWV-estimated and IPWV-radiosonde over Bangalore 2016 at 0000 hr

at 1200 hr. An error of 30% or greater exists in 2.59% cases at 0000 hr and in 1.96% cases at 1200 hr. It is noteworthy that in 8.76% of cases at 0000 hr and 5.51% cases at 1200 hr, the error was less than 1.0%.

The average error is 9.23% and 10.89% at 0000 hr and 1200 hr, respectively. The range of error at 0000 hr is from 0.00% - 64.53%, while at 1200 hr, it varies from 0.008% - 75.76%. The maximum error of 75.76% at 1200 hr, occurred only on 28 October. The maximum error of 64.53% at 0000 hr happened on 27 December. Thus, the estimated IPWV shows a good match with the radiosonde - retrieved precipitable water.

It is noteworthy that on 27 December, at 0000 hr, the $IPWV_{EST}$ (7.19 mm) and $IPW_{GPS}$ (7.8 mm) matched very well, while that retrieved from the radiosonde was only 4.37 mm.

On 28 October at 1200 hr, the $IPWV_{GPS}$ (25.44 mm) and $IPW_{EST}$ (24.20 mm) matched very well, while that retrieved from the radiosonde was only 13.77 mm.

Figs. 4(a&b) show the comparison between the estimated IPWV and the radiosonde-retrieved precipitable water at 0000 hr and 1200 hr, respectively in November 2016. Figs. 4(a&b) reveal a very good match between the two. The two show a good match in most of the months (results not shown). The scatter plot between $IPWV_{EST}$ and the radiosonde-retrieved precipitable water shows a very strong correlation with a correlation coefficient of 0.94 at 0000 hr [Fig. 4(c)] and 0.92 at 1200 hr (result is not shown).

Figs. 5(a&b) respectively show the standard deviations of the estimated IPWV and that retrieved from radiosondeat 0000 hr and 1200 hr. Figs 5(a&b) show a very good match of the standard deviation of the two.

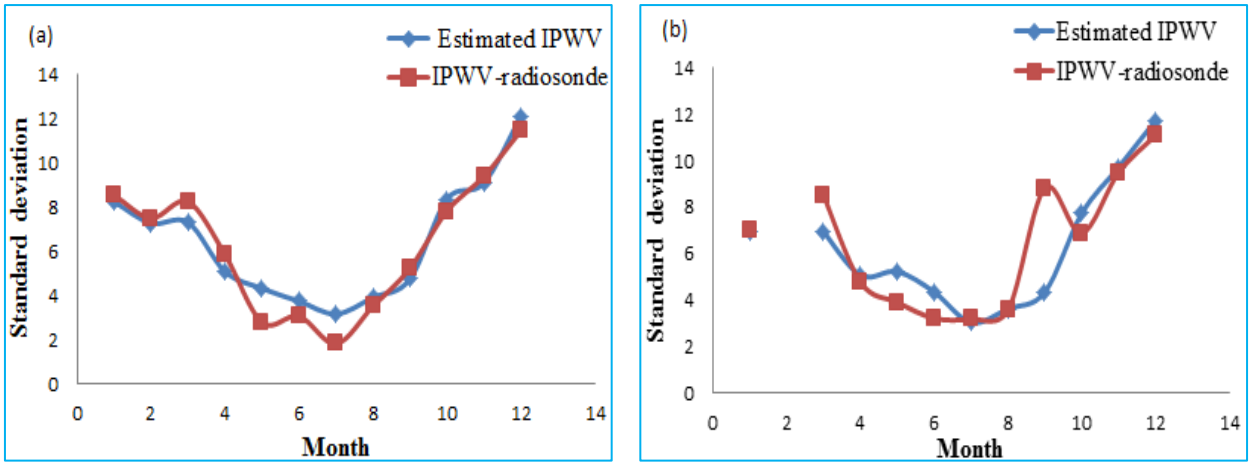


**Figs. 5(a&b).** Standard deviation of estimated and radiosonde retrieved IPWV over Bangalore in 2016 at (a) 0000 hr and (b) 1200 hr

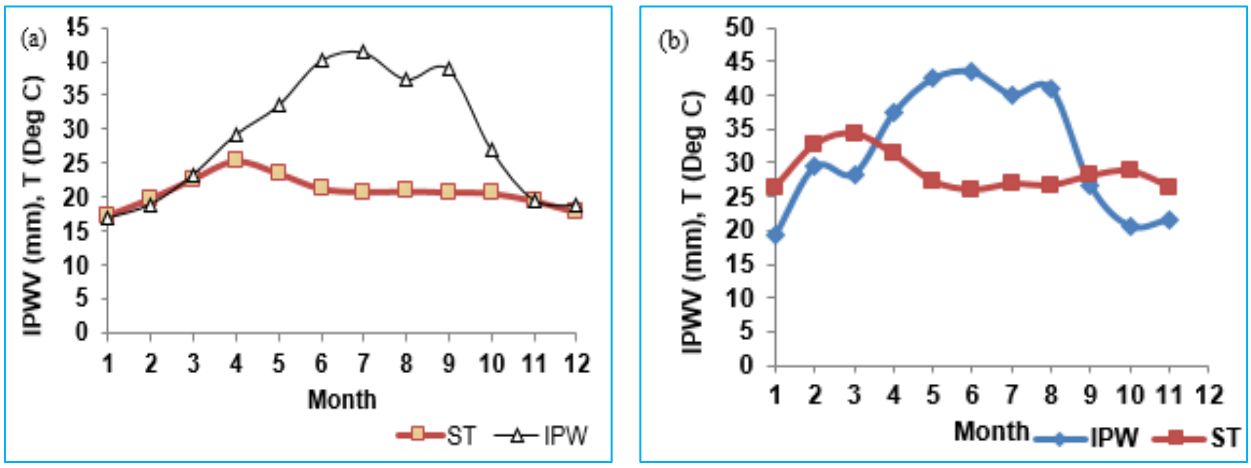


**Figs. 6(a&b).** Monthly variation of IPWV with surface temperature over Bangalore at (a) 0000 hr and (b) 1200 hr

Figs. 5(a&b) reveal that the average standard deviation difference of the two is 0.68 and 0.98 at 0000 hr and 1200 hr, respectively. The range of standard deviation difference varies from 0.23-1.54 and 0.06-4.48 at 0000 hr and 1200 hr, respectively. Smith *et al*. (2006) validated GPS-retrieved IPWV against that recorded by the radiosonde and reported a 2.0 mm standard deviation difference.

### 3.6. *IPWV and surface temperature*

The authors have attempted to find out whether the high (low) IPWV is associated with a high (low) surface temperature. The study shows that the highest (lowest) IPWV value in a month does not necessarily correspond to the highest (lowest) surface temperature [Figs. 6(a&b)].

The daily variations of IPWV and surface temperature reveal that the crests and troughs of these two parameters do not coincide often. The same results are found in all months (results not shown).

To find out the functional relationship between IPWV and surface temperature, if any, the daily IPWV values and the average surface temperature at 0000 hr in a month have been fitted to different models as described in section 2. The validity of the model is judged by the *F*-test at the 5% level of significance. Figs. 7(a&b) respectively show the results of the investigation in September and December at 1200 hr.

Figs. 7(a&b) show that in September and December, a cubic relationship exists between the two. The investigation further shows that the two bear significant correlations in January, February, March, October, November and December ($R^2$ values were 0.51, 0.46, 0.48, 0.43, 0.51 and 0.76 respectively), while in other months, the two do not show any correlations (results not shown). At 1200 hr, only in May, September and

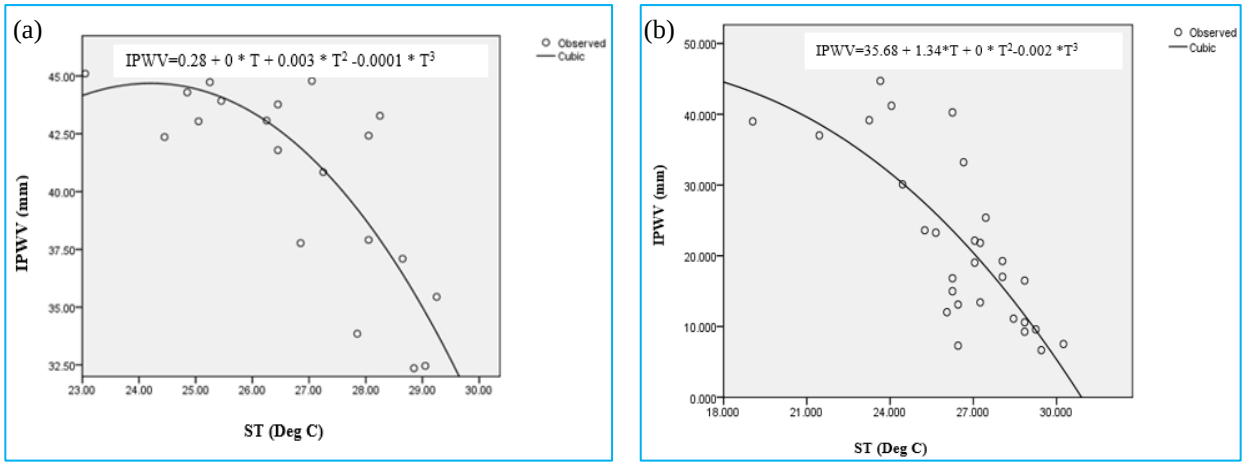


**Figs. 7(a&b).** Variation of IPWV with surface temperature in (a) September at 1200 hr and (b) December at 1200 hr

December, the two show correlations ($R^2$ values being 0.48, 0.65 and 0.62 respectively).

The functional relationship between the two using the daily values for January- December put together does not show any correlation (results not shown).

The monthly average IPWV and surface temperature also do not show any correlations, except at 0000 hr when an insignificant correlation is seen between the two (results not shown). Thus, it appears that from the knowledge of surface temperature alone, IPWV cannot be estimated.

### 3.7. *IPWV and weighted mean temperature ($T_m$)*

Authors have attempted to find out if the weighted mean temperature ($T_m$) bears any correlation with IPWV. For this purpose, they have fitted the daily values of these parameters in a month at 0000 hr and 1200 hr to the curve estimation technique. The study shows that at 0000 hr and 1200 hr, the two bear significant correlations only in November (results not shown). $T_m$ and IPWV do not show any correlations in other months (results not shown).

The investigation also reveals that the highest (lowest) IPWV values do not always correspond to the highest (lowest) weighted mean temperature ($T_m$) values (results not shown).

### 3.8. *IPWV as a function of surface temperature, surface pressure and relative humidity*

The authors attempted to find out the parameters that describe the IPWV. For this purpose, they have investigated the relationship between the IPWV; and surface temperature, surface pressure and relative humidity considering the former as the dependent variable, while the remaining three as the independent ones. They have fitted the daily values of IPWV and those of the other three to different models, as described above. The validity of the model is judged by the F test at a 5% level of significance. The study shows that the IPWV can be better explained in terms of surface temperature, surface pressure and relative humidity, rather than surface temperature alone (results not shown).

The investigation shows that in January, March, September, October and December, a significant relationship exists at both 0000 hr and 1200 hr. In April, May, July and November, significant correlations occur at 1200 hr alone, while in February, a significant correlation is seen at 0000 hr only. It is further noticed that though the correlations between the IPWV and these parameters are better than that considering the surface temperature alone as the controlling factor of IPWV, the $R^2$ values are not very high except in September through January and March. Also, not in all months and at both the hours, a significant correlation is seen. It indicates that some more factors govern the IPWV.

### 3.9. *IPWV and total solar irradiance*

By observing the link between the IPWV and the hour of the day and by realizing the fact that the Sun is the main driving force of the weather and climate on the Earth, the authors aimed to investigate the total solar irradiance (TSI) and its effect on the IPWV. The total solar irradiance is the solar energy incident at the top of the atmosphere. Observation on daily variations of TSI shows that during 2003-2018, in the months of January-June, the maximum TSI ($TSI_{mx}$) always occurs

**TABLE 2(a)**

**IPWV as a function of surface temperature, surface pressure, TSI and relative humidity at 0000 hr**

| S. No. | Month | $R^2$ | Functional relationship |
|---|---|---|---|
| 1. | January | 0.804 | IPWV = -2165.94-2.37SP-0.16RH+6.37ST+3.02TSI |
| 2. | February | 0.607 | IPWV = 2289.08-1.42SP+0.29RH+1.11ST-0.73TSI |
| 3. | March | 0.811 | IPWV = -1593.34+0.7SP+0.16RH+4.58ST+0.63TSI |
| 4. | April | 0.377 | IPWV = -343.20-0.2SP+0.29RH+1.3ST+0.37TSI |
| 5. | May | 0.274 | IPWV = 756.47-1.2SP+0.13RH+0.23ST+0.26TSI |
| 6. | June | 0.344 | IPWV = 1678.31+1.02SP+0.57RH+3.61ST-2.04TSI |
| 7. | July | 0.074 | IPWV = -195.17+0.21SP+0.21RH+0.28ST+0.02TSI |
| 8. | August | 0.214 | IPWV = 501.77-0.28SP+0.13RH+1.71ST-0.2TSI |
| 9. | September | 0.530 | IPWV = 1696.99-1.98SP+0.3RH+1.52ST+0.06TSI |
| 10. | October | 0.637 | IPWV = -544.14+0.29SP+0.49RH+3.63ST+0.14TSI |
| 11. | November | 0.550 | IPWV = -2099.6+3.87SP+0.27RH+0.12ST-1.02TSI |
| 12. | December | 0.832 | IPWV = 3914.18-3.79SP+0.36RH+4.78ST-0.4TSI |
| 13. | January-December (daily data for the whole year) | 0.702 | IPWV = 1119.33-1.03SP+0.31RH+1.01ST-0.15TSI |
| 14. | Monthly avg (January-December) | 0.974 | IPWV = 1715.47-1.78SP+0.7ST-0.51RH-0.01TSI |

**TABLE 2(b)**

**IPWV as a function of surface temperature, surface pressure, TSI and relative humidity at 1200 hr**

| S. No. | Month | $R^2$ | Functional relationship |
|---|---|---|---|
| 1. | January | 0.887 | IPWV = -5761.39-0.54SP+0.77RH+1.97ST+4.4TSI |
| 2. | April | 0.503 | IPWV = 503.34-0.81SP+0.6RH+1.79ST+0.13TSI |
| 3. | May | 0.577 | IPWV = -291.58-0.24SP+0.12RH-1.14ST+0.43TSI |
| 4. | June | 0.327 | IPWV = 1091.93+0.66SP+0.48RH+2.38ST-1.32TSI |
| 5. | July | 0.447 | IPWV = -95.75-0.5SP+0.2RH+0.3ST+0.43TSI |
| 6. | August | 0.443 | IPWV = 652.85-0.29SP+0.18RH+0.24ST-0.28TSI |
| 7. | September | 0.631 | IPWV = 302.45-0.32SP+0.19RH-1.01ST+0.03TSI |
| 8. | October | 0.508 | IPWV = -325.33+0.27SP+0.53RH-0.78ST+0.08TSI |
| 9. | November | 0.880 | IPWV = -688.01+0.7SP+0.82RH+1.71ST+0TSI |
| 10. | December | 0.810 | IPWV = 2636.34-0.47SP+0.38RH-0.24ST-1.57TSI |
| 11. | January-December (daily data for the whole year) | 0.818 | IPWV = 543.59-0.43SP+0.44RH+0.56ST-0.12TSI |
| 12. | Monthly avg (January-December) | 0.966 | IPWV = -1084.17+1.31SP+0.72RH+1.61ST-0.11TSI |

in the beginning of the month, while the minimum TSI ($TSI_{mn}$) occurs at the end of the month (Table 1). During July-December, exactly the opposite effect is seen. It is noteworthy that the $TSI_{mx/mn}$ does not exhibit the above regularity during 1978-2002 (results not shown). The investigation shows that in 2016 the yearly $TSI_{mx}$ occurs on 1 January, while the $TSI_{mn}$ occurs on 3 July. The monthly average $TSI_{mx}$ occurs in January, while the monthly average $TSI_{mn}$ occurs in July.

Table 1 also shows the occurrence of $IPWV_{mx/mn}$ in a month. Table 1 shows that in 2016, sometimes, the IPWV minima dates are very close to the TSI maxima dates. The above regularity between the TSI and the IPWV has

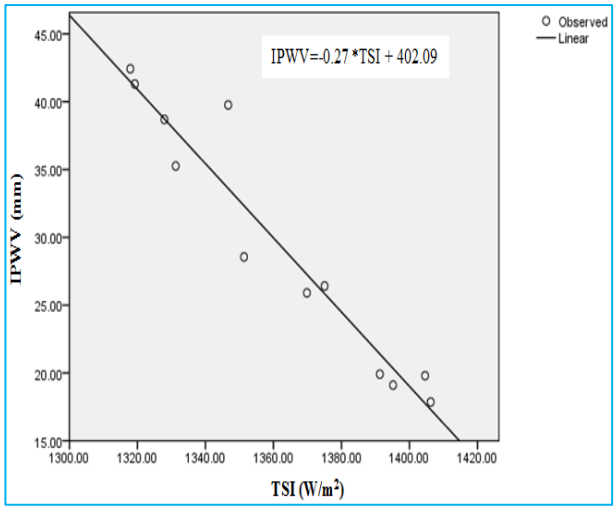


**Fig. 8.** Variation of monthly average IPWV and TSI

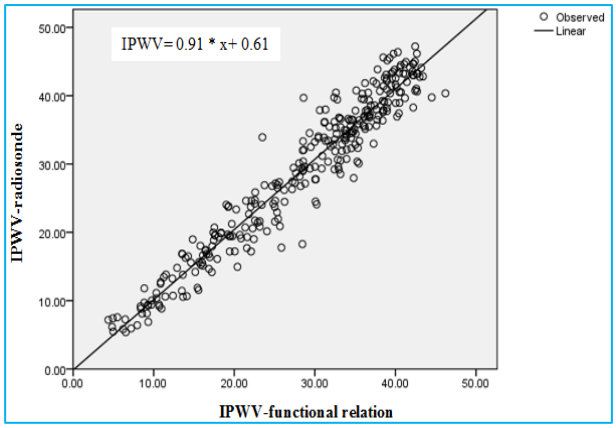


**Fig. 9.** Variation of IPWV-functional relation and IPWV-radiosonde over Bangalore 2016 at 1200 hr

initiated an attempt to find out the correlations between the two, if any. For this purpose, the monthly average values of the TSI and that of the IPWV at 0000 hr have been fitted to different models as described in section 2. The validity of the model is judged by the F test at the 5% level of significance. Fig. 8 shows the result of the analysis. It shows that the two bear very strong correlations. However, no significant correlations existbetween the daily IPWV and TSI (results not shown). The study (Sen Jaiswal *et al.*, 2020d) reveals the correlations between slant tropospheric delay and TSI. As IPWV causes slant tropospheric delay (Emardson and Derks, 2000), this, in turn, implies correlations between IPWV and TSI.

The rotation of the Earth about its axis causes day and night and the revolution of the Earth around the Sun causes season. The daily insolation reaching a particular location on the Earth depends on the rotation and the revolution of the Earth. Thus, it appears that the insolation and in turn, the total solar irradiance affects the precipitable water, which is the manifestation of the Sun-Earth and atmosphere-ocean coupling. The total solar irradiance, in turn, depends on the solar cycle. Thus, it appears that an insight into the solar cycle will undoubtedly elevate the understanding of the precipitable water. This, in turn, will elevate the understanding of the GPS signal delay.

Tables 2(a&b) show the correlations of IPWV as a function of surface temperature, surface pressure, relative humidity and total solar irradiance at 0000 hr and 1200 hr, respectively. Tables 2(a&b) show that IPWV can be better explained as the combination of all four parameters than that by including one or two of these.

### 3.9.1. *Validation of the functional relations of IPWV with SP, ST, RH and TSI*

Authors have validated the IPWV values estimated based on the functional relationships with those measured by the radiosonde. Figs. 4(a&b) show the comparison between the two over Bangalore at 0000 hr and 1200 hr, respectively in November 2016. Figs. 4(a&b) show a good match between the two. In other months also, the two show a good match (result not shown). The analysis in whole 2016 shows less than 10% error in 52.27% cases at 0000 hr and 50.19% cases at 1200 hr. An error of 30% or greater exists in 11.69% cases at 0000 hr and in 9.16% cases at 1200 hr. The average error is 15.01% and 13.31% at 0000 hr and 1200 hr, respectively. Thus, the estimated IPWV based on the functional relations shows a good match with the radiosonde-retrieved precipitable water except in a few cases. Figs. 4(a&b) show the comparison between the estimated IPWV based on the functional relations and the radiosonde-retrieved precipitable water at 0000 hr and 1200 hr, respectively in November 2016. Figs. 4(a&b) reveal a very good match between the two. The two show a good match in most of the month (results not shown). Fig. 9 shows the scatter plot between the radiosonde retrieved IPWV and that based on the functional relationship over Bangalore at 1200 hr in 2016. Fig. 9 shows a correlation coefficient of 0.89 between the two. A correlation coefficient of 0.86 is seen at 0000 hr (result not shown).

Figs. 4(a&b) also show the comparison between the estimated IPWV based on the functional relations and $IPWV_{EST}$ at 0000 hr and 1200 hr, respectively in November 2016. Figs. 4(a&b) reveal a very good match between the two. The two show a good match in most of the month (results not shown). Validation of precipitable water based on the functional relationships with the estimated IPWV shows an error of less than 10% in

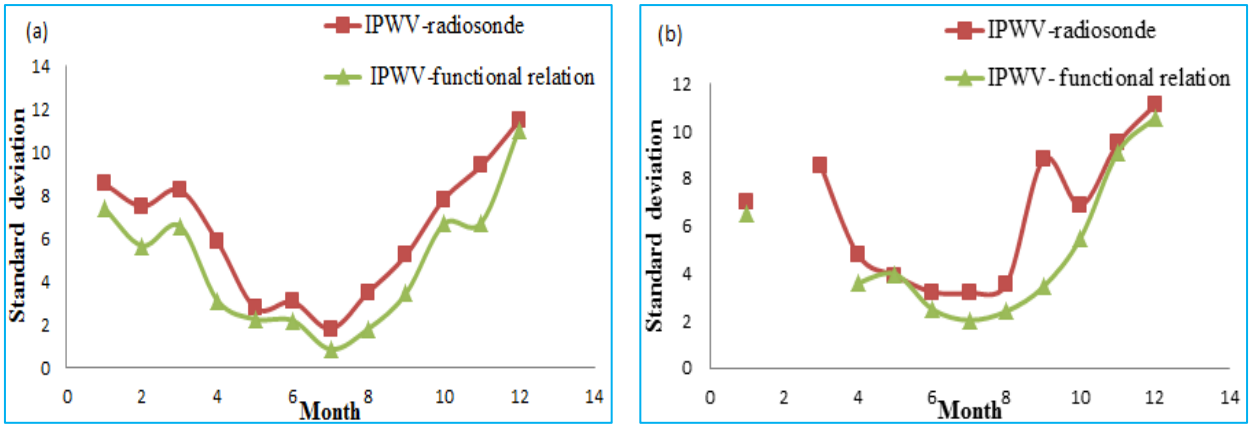


**Figs. 10(a&b).** Standard deviation of radiosonde-retrieved and functional relation-based IPWV over Bangalore in 2016 at (a) 0000 hr and (b) 1200 hr

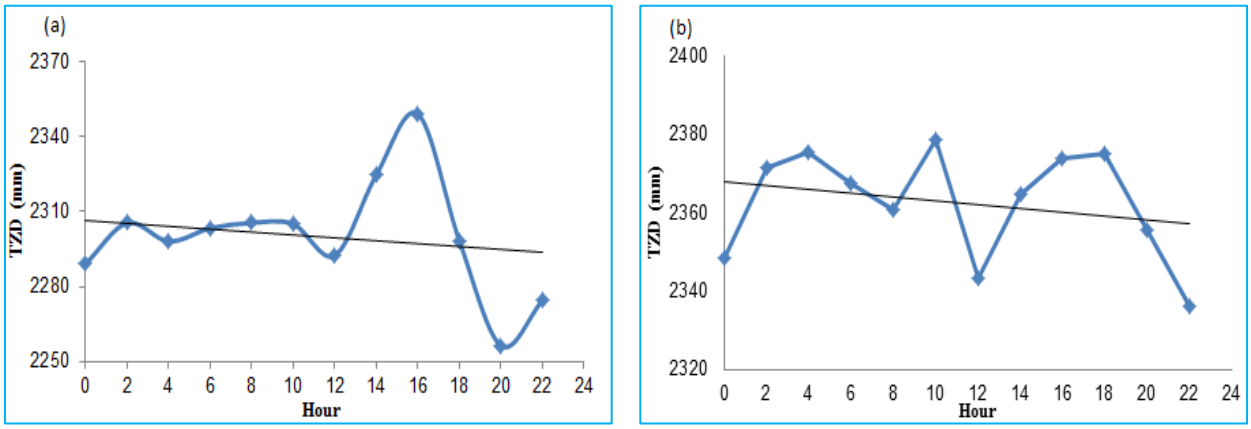


**Figs. 11(a&b).** Diurnal variation of TZD on (a) 1 June 2016 and (b) 1 September 2016

51.13% cases at 0000 hr and 62.89% cases at 1200 hr. An error of 30% or greater is found in 12.22% cases at 0000 hr and 6.25% cases at 1200 hr.

The study of Zhang *et al*. (2016) with co-located GPS stations, radio sounding stations and a sunphotometer station over China indicates a correlation coefficient of greater than 0.98 between the GPS-retrieved and sunphotometer-retrieved IPWV. Kruczyk *et al*. (2017) found a very good correlation between the GPS-retrieved IPWV and that retrieved from the sunphotometer at Belsk, Poland. A comparison of slant integrated water vapor with that measured by a ground-based water vapor radiometer shows a good agreement between the two (Shangguan *et al*., 2015). A comparison of GOES moisture-derived product and GPS-IPW by Birkenheuer and Gutman (2005) over Lamont, Oklahoma shows a strong correlation between the two. The precipitable water retrieved from the MODIS compares well with that retrieved from the GNSS (Mota *et al*., 2019).

Figs. 10(a&b) respectively show the standard deviations of the IPWV values estimated based on the functional relationships and that retrieved from radiosonde at 0000 hr and 1200 hr.

A Comparison of INSAT-3D-derived total precipitable water with radiosonde-observed total precipitable water over India from May to September in 2016 reveals a good match between the two (Parihar *et al*., 2018). However, the standard deviation reported by Parihar *et al*. (2018) is more than that reported in this article. The reason behind the high standard deviation reported by Parihar *et al*. (2018) maybe because of representing results over subdivisions, instead of a particular location.

To find the validity of the functional relations established in this paper for 2016, the authors have estimated the IPWV values over Bangalore in 2018 using these relations. The investigation shows that at 0000 hr, in

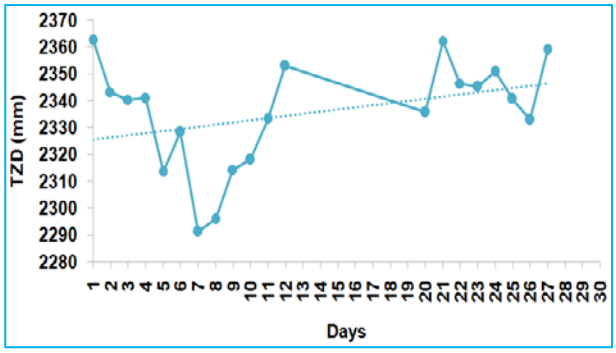


**Fig. 12.** Daily variation of hourly averaged troposphericzenith delay (TZD) over Bangalore in September

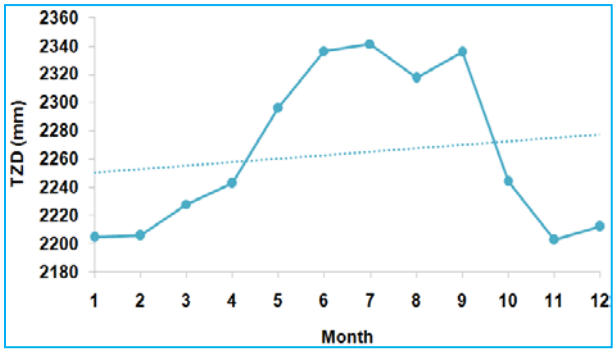


**Fig. 13.** Monthly variation of troposphericzenith delay (TZD) over Bangalore in 2016

51.1% of cases, an error of less than 10% is seen. An error of greater than 30% is seen in only 11.1% of cases at 0000 hr. At 1200 hr, in 4.7% of cases, an error of greater than 30% is seen, while an error of less than 10% is seen in 67.5% of cases. Thus, the functional relations suggested by the authors in this paper appear to estimate IPWV with good accuracy.

### 3.10. *Troposphericzenith delay*

The diurnal variations of troposphericzenith delay (TZD) on 1st June and 1st September in 2016 are shown in Figs. 11(a&b), respectively.

Figs. 11(a&b) show that the TZD attains the highest values at different hours on different days. The trend of diurnal variations is also different on different days. Sometimes an increasing trend exists, while on some other days, a decreasing trend is seen over 0000-2300 hr. Other months also show the same results (results not shown).

The hourly averaged TZD on a day shows variations throughout a month. Fig. 12 shows the variation of hourly averaged TZD in September. Results for other months are not shown.

The daily variations of hourly averaged TZD obtained from the GPS show that during January, March, April, August, October and November, the TZD minima ($TZD_{mn}$) occur by the end of the month, while in February, May, September and December, these occur at the beginning of the month. In June and July, these occur in the middle of the month. In January, June, September and November, the TZD maxima occur at the beginning of the month, while in May and August, these occur by the end of the month. In other months, the TZD maxima ($TZD_{mx}$) occur in the middle of the month (results not shown).

The occurrence of daily $TZD_{mx}$ and $TZD_{mn}$ is shown in Table 1 which shows that at 0000 hr, in March, April, October and November, the $TZD_{mn}$ occurs by the end of the month, while in January, February, May, June and September, it occurs at the beginning of the month. In July, August and December, the $TZD_{mn}$ occurs in the middle of the month.

In February, March, May, October and December, the $TZD_{mx}$ occurs in the middle of the month, while in June, August and September, it occurs by the end of the month. In April, July and November, the $TZD_{mx}$ occurs at the beginning of the month.

Besides, Table 1 shows that the dates of occurrence of $TZD_{mx}$ and $IPWV_{mx}$ mostly coincide. The same holds good for the minima also.

Fig. 13 shows the monthly variation of TZD. It shows that in July the TZD attains the maximum value, while November records the minimum.

### 3.11. *Zenith wet delay (ZWD)*

The investigation shows that as ZWD increases, the IPWV also increases, which is obvious from equation (7).

Figs. 14(a&b) respectively show the daily variation of ZWD and IPWV in July at 0000 hr and 1200 hr. On 14 July 2016, the IPWV value is 37.0 mm and the ZWD is 238.65 mm. This implies that a column of 37.0 mm water vapor causes a delay of an equivalent path length of 238.65 mm to the GPS signal in reaching the Earth station receiver from the satellite.

It is noteworthy that the ZWD and the IPWV show the same trend in diurnal, monthly and daily variations-the crest of one parameter falling on the other and the

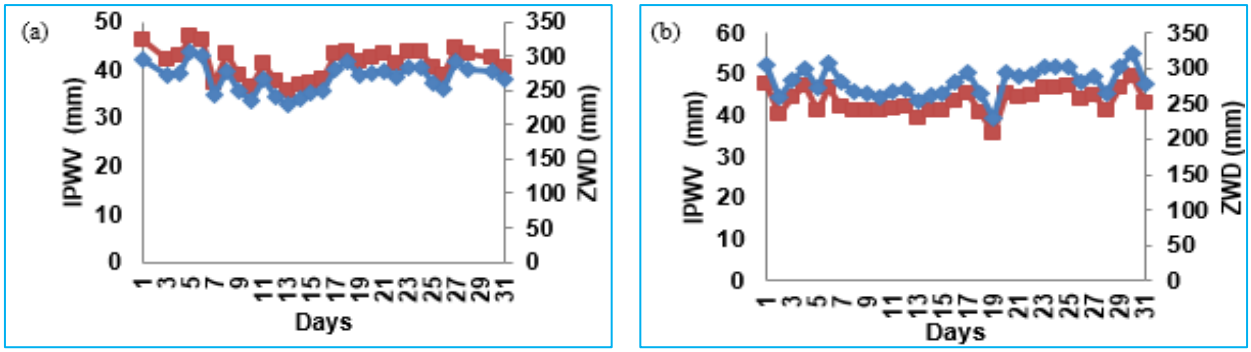


**Figs. 14(a&b).** Daily variation of ZWD and IPWV over Bangalore in July at (a) 0000 hr and (b) 1200 hr

trough of one on the trough on the other (results not shown).

### 3.12. *Weighted mean temperature ($T_m$) over Bangalore*

The weighted mean temperature ($T_m$) shows significant daily variations every month (results not shown). The investigation shows that the $T_m$ at 0000 hr is different from that at 1200 hr. The same results are seen in other months (results not shown). At the 0000 hr and 1200 hr, the $T_m$ attains its maximum value in April, while the minimum value occurs in November (results not shown).

Besides, the investigation shows that at 1200 hr, during January-May, August and September, the $T_m$ shows an increasing trend, while a decreasing trend occurs in daily variations over a month, in June, October, November and December (insignificant) (results not shown). At 0000 hr, an increasing trend happens in daily variations in January-May. In June-November and in December, a decreasing trend exists (results not shown), while in December, an insignificantly decreasing trend is seen.

The monthly averaged $T_m$ at 1200 hr is more than at 0000 hr in March, April, June, October and November. However, in January, May, July, August, September and December, the monthly averaged $T_m$ at 1200 hr is less than that at 0000 hr (results not shown).

### 3.13. *Π analyses over Bangalore*

Π shows significant daily and monthly variations. It shows an increasing trend in some months (January-May) and in some months (June-November), a decreasing trend is seen (results not shown).

At the 0000 hr and 1200 hr, the Π attains the maximum value in April, while the minimum occurs in November. The months of January, April, May, June, August and September shown increasing trend in the daily variations of Π, while in October and December a decreasing trend (insignificant) is seen. In November, at 1200 hr, very little variation in Π is found, implying neither a decreasing nor an increasing trend (results not shown).Besides, the study reveals that the maximum Π occurs in April and the minimum occurs in November.

## 4. Conclusions

The study reports the tropospheric zenith delay (TZD), zenith wet delay (ZWD), $T_m$, Π and integrated precipitable water vapor (IPWV) over Bangalore in the year 2016. The study reveals that IPWV increases with an increase in ZWD. The IPWV shows diurnal, daily and monthly variations. The temperature at a location appears to influence the IPWV. However, the latter is not found to be the sole governing factor of the former. The surface temperature, surface pressure, total solar irradiance and relative humidity, put together, give a better understanding of the IPWV. The monthly average IPWV shows a very strong correlation with the total solar irradiance, indicating the influence of the solar cycle on the IPWV and hence on the wet delay. The validation of the estimated IPWV from GPS and that based on the functional relationships suggested by the authors show a good match with radiosonde-retrived IPWV. However, the match is a little better in the case of the estimated IPWV from GPS. Besides, the functional relations established in this paper for 2016 produced IPWV values in 2018 over Bangalore, with good accuracy. Thus, one can use the approach described in this paper in deriving the functional relations to estimate IPWV over a location where measured values are not available.

*Acknowledgment*

The authors are grateful to Sona College of Technology for providing the infrastructure to carry out the work. The authors convey sincere thanks to the Indian

Space Research Organization, Department of Space, Government of India for sponsoring the work under the NavIC-GAGAN Utilization Program.

*Disclaimer* : The contents and views expressed in this research paper/article are the views of the authors and do not necessarily reflect the views of the organizations we belong to.

**References**


Arnold, N. F. and Robinson, T. R., 1998, "Solar cycle changes to planetary wave propagation and their influence on the middle atmosphere circulation", *Ann. Geophys.*, **16**, 69-76.

Askne, J. and Nordius, H., 1987, "Estimation of tropospheric delay for microwaves from surface weather data", *Radio Sci.*, **22**, 379-386.

Baelen, V. J., Reverdy, M., Tridon, F., Labbouz, L., Dick, G., Bender, M. and Hagen, M., 2011, "On the relationship between water vapour field evolution and the life cycle of precipitation systems", *Q. J. Roy. Meteor. Soc.*, **137**, 204-223.

Bastin, S., Champollion, C., Bock, O., Drobinski, P. and Masson, F., 2007, "Diurnal cycle of water vapor as documented by a dense GPS network in a coastal area during ESCOMPTE IOP2", *J. Appl. Meteorol. Climatol.*, **46**, 167-182.

Battan, L. J. and Kassander, A. R., 1960, "Design of a program of a randomized seeding of orographic cumuli", *J. Meteorol.*, **17**, 583-590.

Benevides, P., Catalao, J. and Miranda, P. M. A., 2015, "On the inclusion of GPS precipitable water vapour in the nowcasting of rainfall", *Nat. Hazards Earth Syst. Sci.*, **15**, 2605-2616.

Bidikar, B., Rao, G. S., Laveti, G. and Kumar, MNVS. S., 2014, "Satellite clock error and orbital solution error estimation for precise navigation applications position", *Sci. Res.*, **5**, 22-26.

Birkenheuer, D. and Gutman, S., 2005, "A Comparison of GOES Moisture-Derived Product and GPS-IPW Data during IHOP-2002", *J. Atmos. Ocean. Technol.*, **22**, 1838-1845.

Brenot, H., Ducrocq, V., Walpersdorf, A., Champollion, C. and Caumont, O., 2006, "GPS zenith delay sensitivity evaluated from high-resolution numerical weather prediction simulations of the 8-9 September 2002 flash flood over southeastern France", *J. Geophys. Res.*, **111**, 1-20.

Brenot, H., Walpersdorf, A., Reverdy, M., Van Baelen, J., Ducrocq, V., Champollion, C., Masson, F., Doerflinger, E., Collard, P. and Giroux, P., 2014, "A GPS network for tropospheric tomography in the framework of the Mediterranean hydrometeorological observatory Cévennes-Vivarais (southeastern France)", *Atmos. Meas. Tech.*, **7**, 553-578.

Byrne, M. P., Pendergrass, A. G., Rapp, A. D. and Wodzicki, K. R., 2018, "Response of the Intertropical Convergence Zoneto climate change : Location, width and strength", *Curr. Clim. Change Rep.*, **4**, 355-370.

Champollion, C., Masson, F., Van Baelen, J., Walpersdorf, A., Chéry, J. and Doerflinger, E., 2004, "GPS monitoring of the tropospheric water vapor distribution and variation during the 9 September 2002 torrential precipitation episode in the Cévennes (southern France)", *J. Geophys. Res.*, **109**, 1-15.

Choudhury, B. J., 1996, "Comparison of two models relating precipitable water to surface humidity using globally distributed radiosonde data over land surfaces", *Int. J. Climatol.*, **16**, 663-675.

Davis, J., Herring, T., Shapiro, I., Rogers, A. and Elgered, G., 1985, "Geodesy by radio interferometry: Effects of atmospheric modeling errors on estimates of baseline length", *Radio Sci.*, **20**, 1593-1607.

Durai, V. R., Roy, S. K. B. and Hatwar, H. R., 2007, "Distribution of precipitable water contents over Indian monsoon region", *MAUSAM*, **58**, 241-250.

Dutta, S. K., Prasad, V. S. and Rajan, D., 2014, "Impact study of integrated precipitable water estimated from Indian GPS measurement", *MAUSAM*, **65**, 461-480.

Eddy, J. A., 1980, "Climate and the role of the Sun", *J. Interdiscip. Hist.*, **10**, 725-747.

Elgered, G., Davis, J. L., Herring, T, A. and Shapiro, I. I., 1991, "Geodesy by radio interferometry : Water vapor radiometry for estimation of the wet delay", *J. Geophys. Res.*, **96**, 6541-6555.

Elliott, W. P. 1995, "On detecting long-term changes in atmospheric moisture", *Clim. Change*, **31**, 349-367.

Emardson, T. R. and Derks, H. J. P., 2000, "On the relation between the wet delay and the integrated precipitable water vapour in the European atmosphere", *Meteorol. Appl*., **7**, 61-68.

Emardson, T. R., Elgered, G. and Johansson, J. M., 1998, "Three months of continuous monitoring of atmospheric water vapor with a network of Global Positioning System receivers", *J. Geophys. Res.*, **103**, 1807-1820.

Engels, S. and Geel, B. V., 2012, "The effects of changing solar activity on climate : Contributions from palaeoclimatological studies", *J. Space Weather. Space Clim.*, **2**, 1-9.

Fujita, M. and Sato, T., 2017, "Observed behaviours of precipitable water vapour and precipitation intensity in response to upper air profiles estimated from surface air temperature", *Nature Sci. Rep.*, **7**, 1-6.

Global Positioning System Standard Positioning Service Signal Specification, 1995, Department of Defense, Washington DC, 1-51.

Haigh, J. D., 2003, "The effects of solar variability on the Earth's climate", *Philos. Trans. R. Soc.*, **361**, 95-111.

Herring, T. A., King, R. W., Floyd, M. A. and McClusky, S. C., 2018, "Introduction to GAMIT/GLOBK", 1-54.

Herring, T. A., Melbourne, T., Szeliga, W., Murray, M. and Phillips, D. A., 2017, "UNAVCO GAGE GPS data analysis plan and products", 1-35.

IGRA website, https://www.ncdc.noaa.gov/data-access/weather-balloon/integrated-global-radiosonde-archive,last accessed 1 March 2021.

Jagannathan, P. and Bhalme, H. N., 1973, "Changes in the pattern of distribution of southwest monsoon rainfall over India associated with sunspots", *Mon. Wea. Rev*., **101**, 691-700.

Junker, W., 2008, "Heavy rainfall forecasting training manual - An ingredients based methodology for forecasting precipitation associated with MCS", HPC Hydrometeorological Testbed/IM Systems Group.

Kruczyk, M., 2015, "Comparison of techniques for integrated precipitable water measurement in the polar region", *Geoinf. Issues*, **7**, 15-27.

Kruczyk, M., Liwosz, T. and Pietruczuk, A., 2017, "Integrated precipitable water from GPS observations and camel sunphotometer measurements at CGOBelsk", *Reports on Geodesy and Geoinfo*., DE GRUYTER, **103**, 46-65.

Kuo, Y. H., Guo, Y. R. and West water, E. R., 1993, "Assimilation of precipitable water measurements into a mesoscale numerical method", *Mon. Wea. Rev.*, **121**, 1215-1238.

Maorong Ge., Calais, E. and Haase, J., 2000, "Reducing satellite orbit error effects in real-time GPS zenith tropospheric delay estimation for meteorology", *Geophys. Res. Lett.*, **27**, 1915-1918.

Manandhar, S., Lee, Y. H., Meng, Y. S. and Ong, J. J., 2017, "A simplified model for the retrieval of precipitable water vapor from GPS signal", *IEEE Trans. Geosci. Remote Sens*., **55**, 6245-6253.

Max, J. R., 2001, "Optical Design Fundamentals for Infrared Systems", 2nd edition, SPIE Press, Bellingham, p206.

Mishra, A. K., 2019, **"**Variability of integrated precipitable water over India in a warming climate", *Meteorol. Appl.*, **27**, 1-4.

Mohanty, U. C., Ramesh, K. J., Kumar, N. M. and Potty, K. V. J., 1994, "Variability of the Indian summer monsoon in relation to oceanic heat budget over the Indian seas", *Dyn. Atmospheres Oceans*, **21**, 1-22.

Mota, G. V., Song, S. and Stepniak, K., 2019, "Assessment of Integrated water vapor estimates from the iGMAS and the Brazilian network GNSS ground-based receivers in Rio de Janeiro", *Remote Sens.*, **11**, 2652-2674.

NOAA website, https://www.ncei.noaa.gov/access/metadata/landing-page/bin/iso?id=gov.noaa.ncdc:C00962, last accessed 13 March 2021.

Parihar, S., Mitra, A. K., Mohapatra, M. and Bhatla, R., 2018, "Potential of INSAT-3D sounder-derived total precipitable water product for weather forecast", *Atmos. Meas. Tech*., **11**, 6003-6012.

Puviarasan, N., Yadav, R., Giri, R. K. and Singh, V., 2020, "GPS Meteorology: Error in the estimation of precipitable water by ground based GPS system in some meso-scale thunderstorms - A case study", *MAUSAM*, **71**, 175-186.

Sen Jaiswal, R., Fredrick, S. R., Thirumala Lakshmi, K., Rasheed, M. and Dobal, R., 2020a, "Global scenario of radar-bright band intensity", *J. Earth Syst. Sci*., submitted on 18 February, 2020.

Sen Jaiswal, R., Neela, V. S., Fredrick, S. R., Rasheed, M., Zaveri, L. and Sowmya, V., 2014, "Identification of convective/ stratiform dominance over surface rainfall", *MAUSAM*, **65**, 219-232.

Sen Jaiswal, R., Siva, M., Rasheed, M. and Thirumala Lakshmi, K., 2020b, "Characteristics of convective/stratiform dominance on surface rainfall over a few tropical locations", *J. Earth Syst. Sci.*, **131**, 1-12.

Sen Jaiswal, R., Vinotha, M., Thirumala Lakshmi, K. and Siva, M., 2020c, "Linking the solar cycle and Earth's climate", *J. Earth Syst. Sci*., submitted on 8 August 2020.

Sen Jaiswal, R., Thirumala Lakshmi, K., Dobal, R. and Siva, M., 2020d, "Study of tropospheric slant delay retrieved from the IRNSS", *Proc. of SPIE*., **11531**, 1-32.

Shangguan, M., Heise, S., Bender, M., Dick, G., Ramatschi, M. and Wickert, J., 2015, "Validation of GPS atmospheric water vapor with WVR data in satellite tracking mode", *Ann. Geophys*., **33**, 55-61.

Shapiro, R., 1975, "The variance spectrum of monthly mean central England temperatures", *Q. J. Roy. Meteor. Soc.*, **101**, 679-681.

Shoji, Y., 2013, "Retrieval of water vapor inhomogeneity using the Japanese nationwide GPS array and its potential for prediction of convective precipitation", *J. Meteorol. Soc. Jpn.*, **91**, 43-62.

Smith, T. L., Benjamin, S. G., Gutman, S. I. and Sahm, S., 2006, "Short-range forecast impact from assimilation of GPS-IPW observations into the rapid update cycle", *Mon. Wea. Rev*., **135**, 2914-2930.

SOlar Radiationand Climate Experiment website, http://lasp.colorado.edu/home/sorce/data/tsi-data/#datafiles, last accessed 10th February, 2019.

Solheim, F. S., Vivekanandan, J., Ware, R. H. and Rocken, C., 1999, "Propagation delays induced in GPS signals by dry air, water vapor, hydrometeors and other particulates", *J. Geophys. Res.*, **104**, 9663-9670.

Solheim, J. E., Stordahl, K. and Humlum, O., 2012, "The long sunspot cycle 23 predicts a significant temperature decrease in cycle 24", *J. Atmos. Sol. Terr. Phys.*, **80**, 267-284.

Soon, W. W. H. and Yaskell, S. H., 2003, "The maunder minimum and the variable Sun-Earth connection", World Scientific Publishing Company, Singapore, p324.

Taylor, K. E. and Ghan, S. J., 1992, "An analysis of cloud liquid water feedback and global climate sensitivity in a General Circulation Model", *J. Clim.*, **5**, 907-919.

Theophrastus, 371-287 BCE, "De Signis Temperstatum" (Enquiry into Plants and Minor Works on Odours and Weather Signs). *Trans. Hort, A.*, **II.**

TRMM data users handbook, 2001, National Space Development Agency of Japan (NASDA), 1-226.

Varma Raja, M. K. R., Gutman, S. I., Yoe, J. G., Mcmillin, L. M. and Zhao, J., 2008, "The validation of AIRS retrievals of integrated precipitable water vapor using measurements from a network of ground-based GPS receivers over the contiguous United States", *J. Atmos. Ocean. Technol*., **25**, 416-428.

Webster, P. J., Magana, V. O., Palmer, T. N., Shukla, J., Tomas, R. A., Yanai, M. and Yasunari, T., 1998, "Monsoons: Processes, predictability and the prospects for prediction", *J. Geophys. Res.*, **103**, 14451-14510.

Yan, X., Ducrocq, V., Poli, P., Hakam, M., Jaubert, G. and Walpers-dorf, A., 2009, "Impact of GPS zenith delay assimilation on convective-scale prediction of Mediterranean heavy rainfall", *J. Geophys. Res.*, **114**, 1-15.

Zhai, P. and Eskridge, R. E., 1997, "Atmospheric water vapor over China", *J. Clim.*, **10**, 2643-2652.

Zhang, H., Yuan, Y., Li, W., Ou, J., Li, Y. and Zhang, B., 2017, "GPS PPP-derived precipitable water vapor retrieval based on Tm/Ps from multiple sources of meteorological data sets in China", *J. Geophys. Res.*, **122**, 1-19.